Transient heating and melting transformations in argon-ion laser irradiation of polysilicon films

Xianfan Xu, Scott L. Taylor, Hee K. Park, and Costas P. Grigoropoulos
Department of Mechanical Engineering, University of California, Berkeley, California 94720

(Received 29 July 1992; accepted for publication 19 February 1993)

Undoped, thin silicon films have been deposited at different temperatures on fused quartz substrates by low-pressure chemical vapor deposition. The heating of these films by continuous wave, argon-ion laser beam irradiation has been studied. *In situ*, normal incidence reflectivity measurements have been obtained at specified locations in the semiconductor films. Melting and recrystallization phenomena have been probed by transient measurements. The static film reflectivity at elevated temperatures, up to about 1400 K, has also been measured. The temperature field has been analyzed numerically, using a modified enthalpy model. Thin-film optics were used to calculate the argon-ion laser light absorption in the polysilicon layer and the transient reflectivity response to the probing laser light. The predicted and experimentally measured reflectivity histories have been compared. The initial stages of the phase change process have been captured by high-speed photography.

I. INTRODUCTION

Polycrystalline silicon (polysilicon) is used in the electronics industry as gate metal in metal-oxide-semiconductor (MOS) transistors.[1] Advances in electronic film deposition and in selective etching techniques have enabled the emergence of a new class of micromechanical devices, sensors, and actuators.[2] Thermal annealing of the thin film can reduce stresses induced by the deposition process,[3] which may cause buckling and even fracture of the thin film. Recrystallization of semiconductor films has been shown to improve the electrical transport properties and the reliability of electronic devices.[4] The use of light sources to melt and subsequently recrystallize thin semiconductor layers on insulators, such as oxidized wafers and bulk amorphous substrates, has shown good potential for applications to commercial very large scale interaction (VLSI) technology.[5] The crystal growth may be controlled by modifying the laser beam shape.[6] The annealing laser beam geometry affects the induced temperature field. Knowledge of the temperature distribution in laser-annealed thin silicon films is essential for successful material processing.

The temperature distribution in the thin film is controlled by the laser power, the distribution of laser beam intensity, and the sample translation speed. Models of silicon film annealing by infinitely extensive laser line sources have utilized the enthalpy method for the solution of phase change problems.[7] A three-dimensional transient numerical algorithm for the laser melting and recrystallization of thin silicon films has been presented.[8] The results of this method have been compared with experimental data on the steady-state size of the formed molten pools. The numerical technique has been improved[9,10] by eliminating the assumption of constant temperature for the mesh elements that contain the melt front. This modified enthalpy method combines the energy balance approach with direct tracking of the interface boundary in a fixed rectangular computational domain.

This work studies the transient heating of thin polysilicon films by argon-ion laser beams. Localized, *in situ* reflectivity measurements capture the dynamics of the laser-semiconductor interaction, which occurs at the millisecond timescale. The static, solid phase silicon film reflectivity is measured in an inert gas environment at elevated temperatures, up to 1400 K. High-speed photographic observations reveal that the initial film melting occurs through an oscillatory, nonhomogeneous process. It is noted that partial melting has been observed in steady-state thin silicon films heated by visible[8,11,12] and infrared laser light sources.[13] The experimental measurements are compared to numerical results that are obtained using the modified enthalpy method.

II. EXPERIMENTAL PROCEDURE

The experiment is performed on samples of the type shown in Fig. 1. Undoped polysilicon layers are deposited on fused quartz substrates. The substrates have a thickness, d_s=0.5 mm. The silicon films were prepared from pure silane in a front-injection, low-pressure chemical vapor deposition (LPCVD) furnace, at average chamber temperatures of 580 and 630 °C and at a silane pressure of 300 mTorr. Annealing at a temperature of 1050 °C in a dry N_2 atmosphere was performed for a period of 30 min. The polysilicon layer thickness was measured optically by scanning interferometry. Roughness measurements were performed using an Alphastep 200 automatic profilometer. Samples were capped by LPCVD deposited 0.5-μm-thick SiO_2 layers, while uncapped samples were also retained for each of the above-mentioned deposition temperatures. The thickness of the capping layer was approximated by measuring the oxide thickness deposited on dummy, single crystalline wafers using ellipsometry. Results of the thickness and roughness measurements are summarized in Table I.

The samples were processed using the apparatus shown in Fig. 2. The annealing beam was produced by a

 0021-8979/93/128088-09$06.00

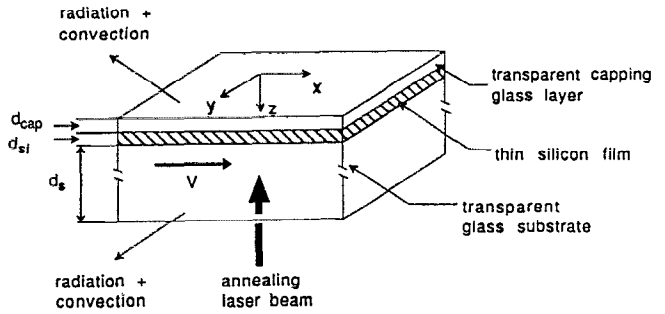

FIG. 1. Structure of the sample used during these experiments.

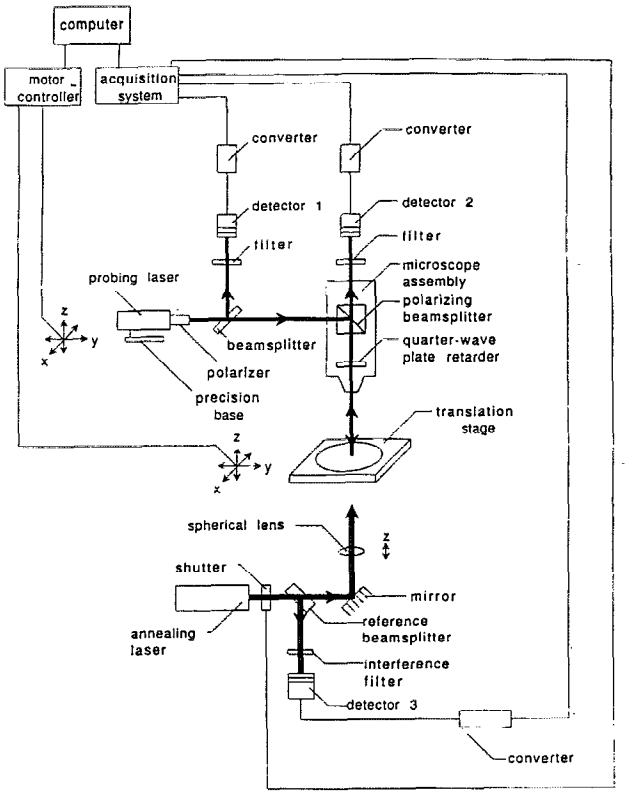

FIG. 2. Schematic of the laser annealing apparatus.

continuous-wave (cw) argon-ion laser. The laser was used as a single line source with a wavelength $\lambda = 514.5$ nm. The maximum power associated with this wavelength is about 2.5 W. The laser operates in the TEM_{00} mode and the output beam has a Gaussian intensity distribution. A beamsplitter is used to provide a reference signal corresponding to the annealing laser beam power. Measurement of the reference signal shows that the beam is completely unobstructed after about 0.2 ms. The laser is focused by a spherical lens with a focal length of 7 cm. The annealing laser power incident on the sample is calibrated to the reference signal using a thermopile detector.

The $1/e$ irradiance radius of the annealing beam was measured after it passed through the spherical lens (Fig. 3). These measurements were obtained using a rotating chopper technique. A Gaussian laser beam envelope, defined by a minimum beam radius and a focal waist position was fitted by a least-squares error minimization to the experimental data. The radius of the focal waist on the Gaussian fit is 19.3 μm. The experimentally measured minimum beam radius was 17.4 μm. Point by point comparison of experimental data showed a variation of $\pm 7\%$.

Normal incidence reflectivity measurements[14] are made using the setup shown in Fig. 2. A HeNe laser is used as the probing beam. This source emits at a wavelength $\lambda = 632.8$ nm. The probing beam is focused on the sample by a $30\times$ microscope objective lens with a focal length of 6 mm. Using experimental techniques and Gaussian laser beam theory, the $1/e$ irradiance radius corresponding to the focal waist was determined to be 4.3 μm. As a result, the spatial resolution of the microprobe is about 9 μm. The localized reflectivity measurement experiments were performed with the sample placed at the focal waist of the probing laser beam. The entire reflectivity microprobe can be moved on a plane parallel to the sample by two piezoelectric motors. The repeatable positioning accuracy of these motors is 1 μm. Signals from the reflected light, detector 2, and the annealing laser beam reference, detector 3, are measured by a digitizing oscilloscope. The probing laser beam reference, detector 1, is measured using the high-speed voltmeter accessory of a data acquisition con-

TABLE I. Sample parameters.

	Deposition temperature (°C)			
	580		630	
	uncapped	capped	uncapped	capped
Polysilicon thickness (Å)	6190±74	6055±62	6208±50	5944±59
Polysilicon roughness (Å)[a]	35	35	45	45
Capping layer thickness (Å)		4894±326		4864±134

[a]rms roughness, on 50 μm scan lines.

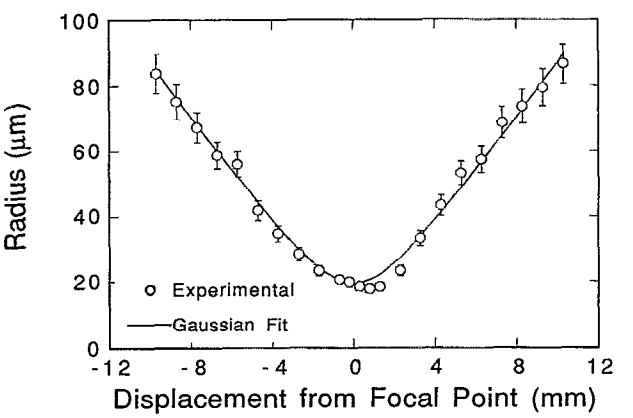

FIG. 3. Radius of the annealing laser beam as a function of the distance from the focal waist.

trol unit. The acquisition frequency for both devices is set to 100 kHz. A computer controller uses internal triggering commands and a two-channel function generator to simultaneously trigger the electronic shutter and the data acquisition hardware. The accuracy of the reflectivity microprobe apparatus was checked by measuring the reflectivity of oxidized crystalline silicon samples. These wafers were well characterized by ellipsometry. The reflectivity of the samples was measured by placing a HeNe laser head at a distance of about 2 m from the sample. The HeNe laser beam was incident on the sample at a small angle ($\sim 0.5°$) with respect to the normal to the sample surface. These measurements and the reflectivity microprobe measurements were in close agreement (absolute reflectivity deviation within 0.005).

Thin-film optical theory is used to derive the optical properties of the sample structure. The encapsulation layer and the polysilicon film are sufficiently thin for wave optics to be important. The substrate, however, has a large thickness to wavelength ratio, d_s/λ, so that light interference effects in that region are smoothed out by variations of the substrate thickness and flatness. Electromagnetic wave interference must therefore be considered in the thin films, while light reflection and transmission in the substrate can be modeled using ray tracing. The following expressions for reflectivity $\mathscr{R}_s^+$ and transmissivity $\mathscr{T}_s^+$ are obtained for a bare substrate, in the case of normal incidence:

$$\mathscr{R}_s^+ = \mathscr{R}_{1s} + \frac{\mathscr{R}_{s2}\mathscr{T}_{1s}\mathscr{T}_{s1}}{1-\mathscr{R}_{s1}\mathscr{R}_{s2}}, \tag{1a}$$

$$\mathscr{T}_s^+ = \frac{\mathscr{T}_{1s}\mathscr{T}_{s2}}{1-\mathscr{R}_{s1}\mathscr{R}_{s2}}. \tag{1b}$$

In the above, $\mathscr{R}_{ij}$ is the reflectivity at the interface of the media i,j:

$$\mathscr{R}_{ij} = \frac{(n_i-n_j)^2}{(n_i+n_j)^2}, \tag{2a}$$

$$\mathscr{T}_{ij} = 1-\mathscr{R}_{ij}, \tag{2b}$$

for $i,j=1$ (region above the top sample surface), 2 (region below the bottom substrate surface), or s (substrate region). The superscript $(+)$ indicates light incident onto the top surface of the thin films. The refractive indices $n_1=n_2=1$, while the substrate is transparent for the annealing and probing laser light wavelengths, having a real refractive index, n_s.

The characteristic transmission matrix $\mathscr{M}_j$ (Refs. 15 and 16), representing an absorbing thin layer of thickness d_j, and having a complex refractive index, $\hat{n}_j$ is given by

$$\mathscr{M}_j = \begin{bmatrix} \cos\left(\frac{2\pi}{\lambda}\hat{n}_j d_j\right) & -\frac{i}{\hat{n}_j}\sin\left(\frac{2\pi}{\lambda}\hat{n}_j d_j\right) \\ -i\hat{n}_j \sin\left(\frac{2\pi}{\lambda}\hat{n}_j d_j\right) & \cos\left(\frac{2\pi}{\lambda}\hat{n}_j d_j\right) \end{bmatrix}. \tag{3}$$

In the above, λ is the laser light wavelength and i is the imaginary unit.

The two-layer transmission matrix $\mathscr{M}_f^+$ for light emanating from region 1 is

$$\mathscr{M}_f^+ = \mathscr{M}_{\text{cap}} \times \mathscr{M}_{si}. \tag{4}$$

The reflection and transmission coefficients r_f^+ and $t_{r,f}^+$ are

$$r_f^+ = \frac{[\mathscr{M}_f^+(1,1)+\mathscr{M}_f^+(1,2)n_s]-[\mathscr{M}_f^+(2,1)+\mathscr{M}_f^+(2,2)n_s]}{[\mathscr{M}_f^+(1,1)+\mathscr{M}_f^+(1,2)n_s]+[\mathscr{M}_f^+(2,1)+\mathscr{M}_f^+(2,2)n_s]}, \tag{5a}$$

$$t_{r,f}^+ = \frac{2}{[\mathscr{M}_f^+(1,1)+\mathscr{M}_f^+(1,2)n_s]+[\mathscr{M}_f^+(2,1)+\mathscr{M}_f^+(2,2)n_s]}. \tag{5b}$$

The film reflectivity and transmissivity in terms of r_f^+ and $t_{r,f}^+$ follow:

$$\mathscr{R}_{1fs} = |r_f^+|^2, \tag{6a}$$

$$\mathscr{T}_{1fs} = n_s|t_f^+|^2. \tag{6b}$$

Let $\mathscr{R}_{sf1}$ and $\mathscr{T}_{sf1}$ be the two-film reflectivity and transmissivity, but for light propagating in the substrate-film-air direction. Equations (1a) and (1b) then yield the following expressions for the structure total reflectivity and transmissivity:

$$\mathscr{R}_{\text{total}}^+ = \mathscr{R}_{1fs} + \frac{\mathscr{R}_{s2}\mathscr{T}_{1fs}\mathscr{T}_{sf1}}{1-\mathscr{R}_{sf1}\mathscr{R}_{s2}}, \tag{7a}$$

$$\mathscr{T}_{\text{total}}^+ = \frac{\mathscr{T}_{1fs}\mathscr{T}_{s2}}{1-\mathscr{R}_{sf1}\mathscr{R}_{s2}}. \tag{7b}$$

The annealing laser beam is incident on the bottom surface of the substrate. The substrate reflectivity ($\mathscr{R}_s^-$) can be calculated using ray tracing:

$$\mathscr{R}_s^- = \mathscr{R}_{2s} + \frac{\mathscr{R}_{s1}\mathscr{T}_{2s}\mathscr{T}_{s2}}{1-\mathscr{R}_{s2}\mathscr{R}_{s1}}. \tag{8}$$

The total reflectivity is obtained by replacing $\mathscr{R}_{s1}$ with $\mathscr{R}_{sf1}$, which corresponds to light propagation in the polysilicon/SiO_2 structure:

$$\mathscr{R}_{\text{total}}^- = \mathscr{R}_{2s} + \frac{\mathscr{R}_{sf1}\mathscr{T}_{2s}\mathscr{T}_{s2}}{1-\mathscr{R}_{s2}\mathscr{R}_{sf1}}. \tag{9}$$

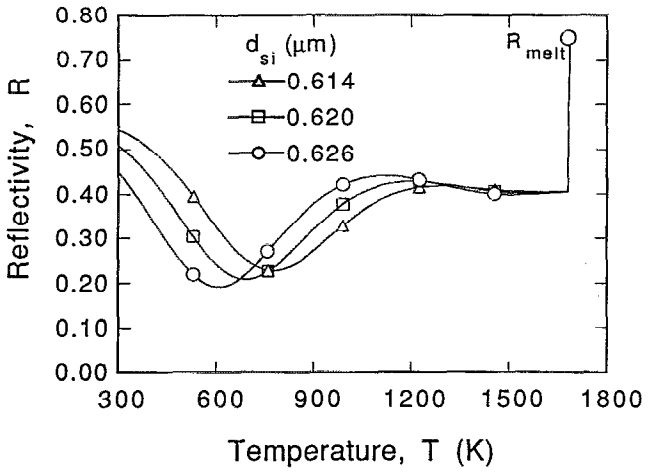

FIG. 4. Calculated normal incidence reflectivity $\mathscr{R}$ of the d_{si}=0.62-μm-thick, uncapped sample, as a function of the silicon layer temperature for the probing laser beam (λ=632.8 nm).

In the above, the superscript (−) indicates light incident onto the bottom surface of the substrate. Experimental data for the complex refractive index of solid, single crystalline silicon in the bulk form[17] were used in predictions of the sample optical properties. The reflectivity as a function of temperature for a 0.62-μm-thick, uncapped sample is shown in Fig. 4. This figure also shows that the sample reflectivity is very sensitive to variations of the silicon layer thickness. Variations of the silicon layer thickness by ±60 Å change the room temperature reflectivity by ∓10%, and produce a shift of the temperature for minimum reflectivity by ∓200 K. There is a discontinuous change in the optical properties upon melting. The bulk liquid silicon complex refractive index[18] is used to determine the optical properties of molten silicon. Reflectivity values of 0.57 and 0.75 are expected for the capped and uncapped thin silicon film upon irradiation by the probing laser.

The apparatus for static, normal incidence reflectivity measurements at high temperatures is shown in Fig. 5. The sample is mounted on a graphite susceptor of 1 in. diameter, heated by a computer-controlled induction heating coil. The temperature of the stage is measured by a Pt-30%Rh/Pt-6%Rh (*B*-type) thermocouple. The uniformity of the sample temperature was verified by measuring the temperature at different locations. The chamber is evacuated to a pressure of 10^{-2} Torr and is backfilled with argon gas. The reflectivity probe is a low-power (1 mW) HeNe laser (λ=632.8 nm). An optical chopper is used to modulate the laser beam signal to a given frequency, thus avoiding detection of the significant thermal emission from the sample and the graphite susceptor. The detector 4 measures a reference signal that yields the instantaneous power of the probing laser. The reflected beam is transmitted through the polarizing beamsplitter to the silicon diode detector 5. Red light interference filters at 632.8 nm are used to block stray light to the detectors 4 and 5. The signals of these two detectors yield the normal incidence reflectivity of the sample, with proper account of the reflectivity by the chamber port fused silica window. The HeNe laser spot area on the sample surface is about 1 mm

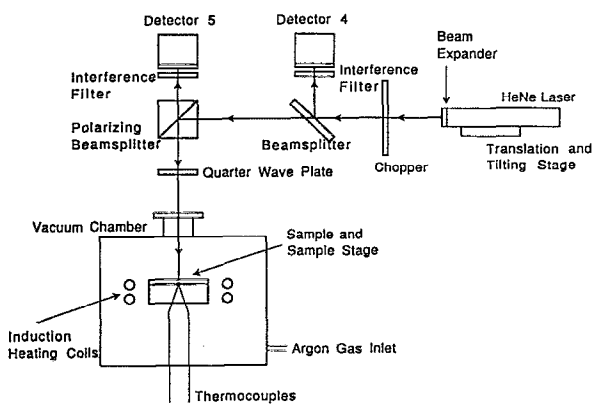

FIG. 5. Schematic of the experimental apparatus for measurement of the static normal incidence reflectivity at high temperatures.

TABLE II. Sample optical properties.

Deposition temperature (°C)	d_{si} (μm)	$\mathscr{R}$	$\mathscr{T}$	$\hat{n}$
580, annealed	0.62	0.51	0.29	3.92+*i*0.032
630, annealed	0.62	0.33	0.33	3.99+*i*0.044

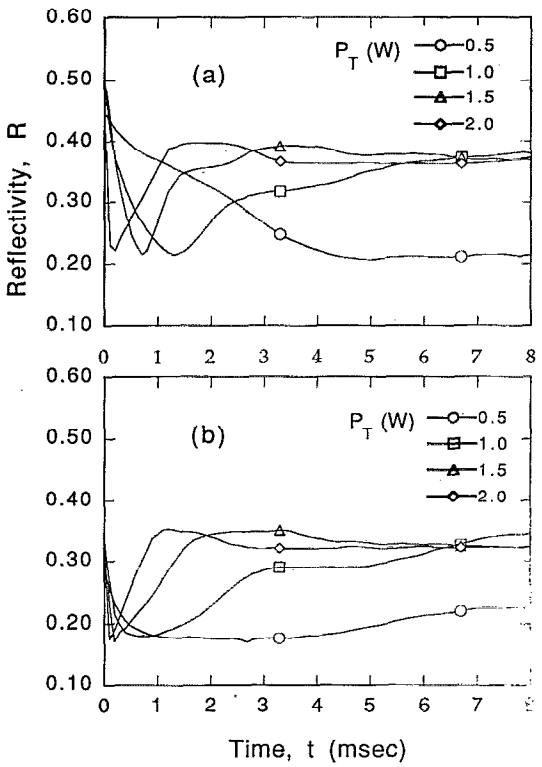

FIG. 6. Transient reflectivity responses of the d_{si}=0.62-μm-thick, uncapped, annealed sample to irradiation by an argon-ion laser beam with W=60 μm and different laser beam powers. The polysilicon deposition temperature is (a) 580 °C and (b) 630 °C.

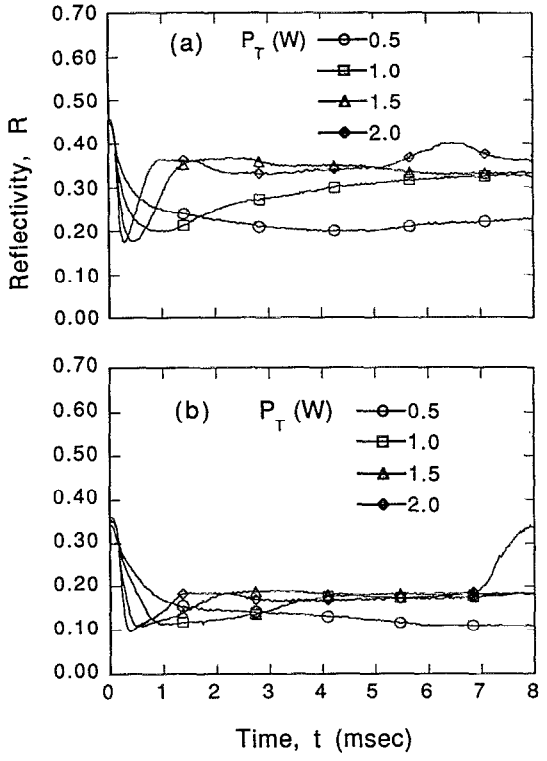

FIG. 7. Transient reflectivity responses of the d_{si}=0.60-μm-thick, capped, d_{cap}=0.50 μm, annealed sample to irradiation by an argon-ion laser beam with W=60 μm and different laser beam powers. The polysilicon deposition temperature is (a) 580 °C and (b) 630 °C.

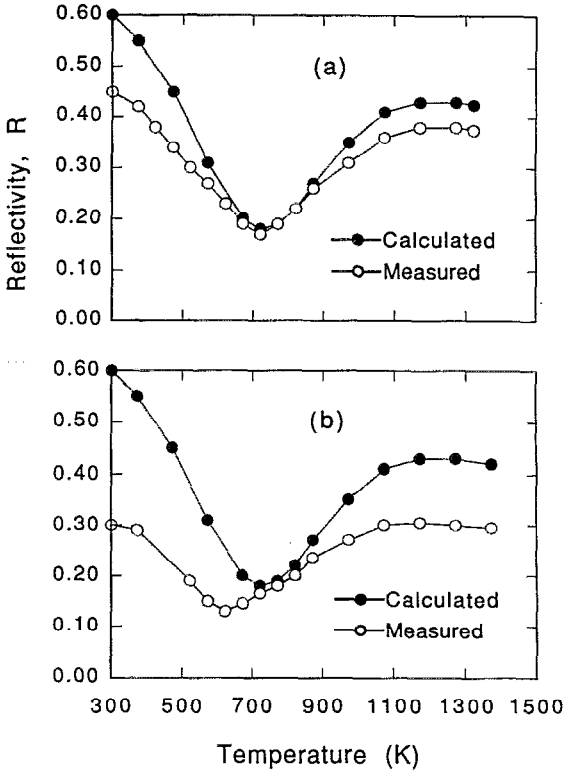

FIG. 8. Experimentally measured (indicated by m), static reflectivities of uncapped samples deposited at (a) 580 °C and (b) 630 °C as functions of temperature vs predicted values (indicated by c) for a d_{si}=0.62-μm-thick silicon layer.

in diameter, thus much larger than the 9-μm-diam spot size of the reflectivity probe shown in Fig. 2. It is noted that the transient heating experiments were conducted on sample regions where the static reflectivity had been measured as discussed in this paragraph.

III. RESULTS

The complex refractive index of the silicon film was obtained at room temperature, from reflectivity $\mathscr{R}$ and transmissivity $\mathscr{T}$ measurement, using the optics model mentioned in the preceding section, and an iterative approximating procedure. The effect of a native oxide layer of thickness up to 50 Å on the film optical properties is negligible. The results are summarized in Table II. For comparison, it is recalled that the single crystalline silicon complex refractive index at a wavelength λ=632.8 nm and at a temperature T=300 K is $\hat{n}_{c\text{-}si}=3.88+i0.02$. The measured value of the as-deposited and annealed silicon film complex refractive index is consistent with reported results.[19–22] These investigations have shown that the complex refractive index is a strong function of the deposition conditions and the post-processing annealing procedure. It is also known that polysilicon films may be modeled as mixtures of void fractions, amorphous and single crystalline components using effective medium theory.[23] The relative phase weights vary with the deposition conditions.

Normal incidence reflectivity measurements have been obtained with the optical microprobe placed at the center of the annealing laser beam. Results are presented for capped and uncapped films (Figs. 6 and 7 correspondingly), deposited by LPCVD, at deposition temperatures 580 and 630 °C. These films are subjected to irradiation by a laser beam with $1/e$ irradiance radius W=60 μm and total powers P_T=0.5, 1.0, 1.5, and 2.0 W. Experimentally

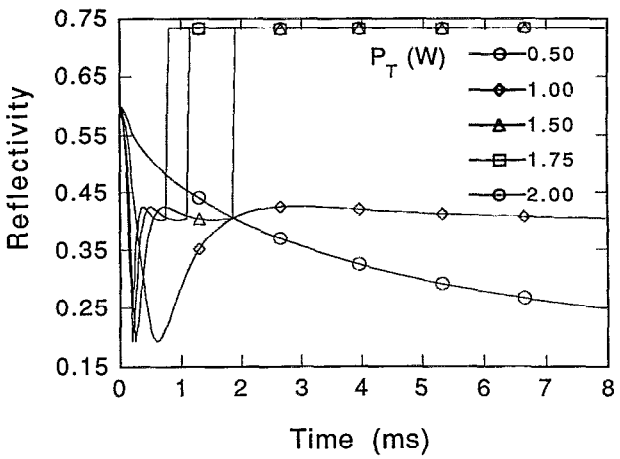

FIG. 9. Predicted transient reflectivity at the center of the heating laser beam for uncapped samples of thickness d_{si}=0.62 μm.

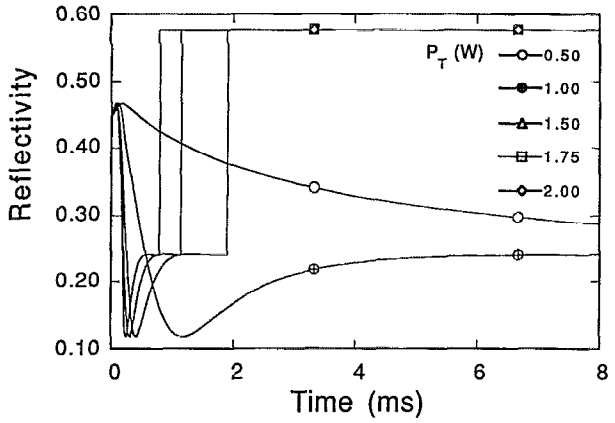

FIG. 10. Predicted transient reflectivity at the center of the heating laser beam for capped samples of thickness $d_{si}=0.60$ μm, $d_{cap}=0.50$ μm.

measured, static, normal incidence reflectivities for both capped and uncapped samples are given in Figs. 8(a) and 8(b). Predicted film reflectivities based on the data for the complex refractive index of bulk silicon[17] are also shown in the same figure. It can be seen that the normal incidence reflectivity for the 580 °C-deposited film approaches more closely the crystalline silicon behavior. Examination of Fig. 6 versus Fig. 8 shows that the transient signals exhibit the trends shown by the static measurement. Moreover, the

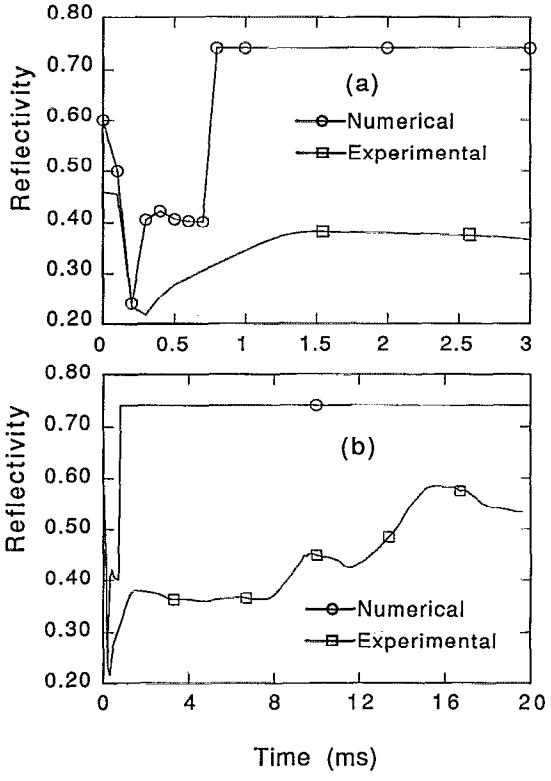

FIG. 11. Comparison between experimental and computed transient reflectivities for the uncapped, $d_{si}=0.62$ μm sample, irradiated by an argon-ion laser beam with $W=60$ μm, $P_T=2.0$ W: (a) over 3 ms and (b) over 20 ms.

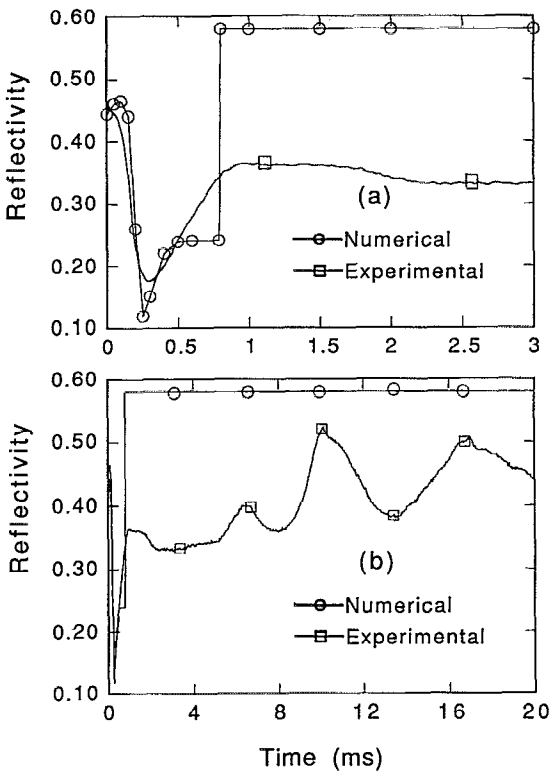

FIG. 12. Comparison between experimental and computed transient reflectivities for the capped, $d_{si}=0.60$ μm, $d_{cap}=0.50$ μm sample, heated by an argon-ion laser beam with $W=60$ μm, $P_T=2.0$ W: (a) over 3 ms and (b) over 20 ms.

correspondence of the room-temperature reflectivity, the minimum reflectivity, and the value of the high-temperature reflectivity plateau is reasonable.

The heat transfer in the silicon film during the irradiation by the laser beam is calculated using a modified enthalpy model.[10,24] The predicted transient reflectivity responses at the center of the annealing laser beam for the laser beam parameters of Figs. 6 and 7 for uncapped and capped samples are shown in Figs. 9 and 10, respectively. Phase change for $W=60$ μm is experimentally observed for a laser beam power $P_T=2.0$ W. The comparison between the experimental and computed reflectivities for uncapped and capped samples is shown in Figs. 11 and 12. On the experimental signal, the transition to melting is not marked by a sharp increase to the liquid silicon value. A positive slope of the reflectivity signal with time is expected, due to the finite size of the probing laser beam, but the observed oscillatory trend of the reflectivity signal is a new finding.

Samples of 0.5 μm thickness were also tested. Figure 13 shows the measured static, temperature-dependent reflectivity for capped polysilicon samples, with $d_{si}=0.5$ μm, $d_{cap}=0.5$ μm. Comparisons of the experimental and computational results for this type of film, using laser processing parameters of $W=60$ μm and $P_T=1.8$ W and 1.4 W are shown in Figs. 14 and 15, respectively. The change in the behavior of the experimental signal at about 2.0 ms matches with the predicted onset of melting. This sample,

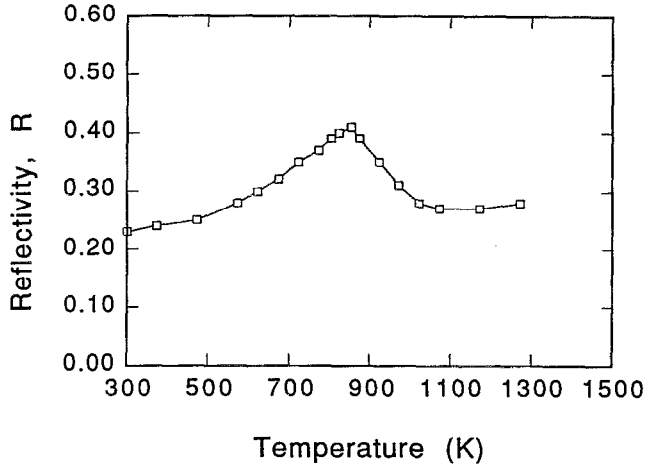

FIG. 13. Experimentally measured temperature dependence of the static reflectivity of the capped, $d_{si}=0.50$ μm, $d_{cap}=0.50$ μm, polysilicon sample.

like all the others tested, showed transition to melting through a periodic process.

The observed oscillatory trend of the reflectivity signal when change of phase occurs is very interesting. The temporal width of the successive reflectivity peaks increases progressively with time, till a steady reflectivity value is established. The oscillatory behavior occurs on the millisecond timescale, and is more pronounced and persisting for lower powers. Figure 16 shows a sequence of high-speed microscopy photographs of the melting process, for $P_T=1.8$ W, $W=60$ μm, corresponding to the reflectivity curve of Fig. 14. The solid-state camera recorded the visible thermal radiation emitted from the samples, with the acquisition speed set at 1 frame/ms. Solid silicon at temperatures close to the melting temperature has a higher emissivity than liquid silicon. Thus, bright regions in the heated spot represent solid silicon, while darker regions correspond to molten material. The photographs initially show a ring of molten material ($t=2$ ms), which appears to grow in area ($t=6$ ms). At $t=8$ ms, a substantial part of the heated zone returns to the solid phase, then remelts at $t=14$ ms. The partial melting/recrystallization cycle is repeated, yielding an increased solid phase fraction at $t=18$ ms. The same trend but with a smaller heat affected zone was observed for a laser power $P_T=1.4$ W (Fig. 17), corresponding to the transient reflectivity measurement shown in Fig. 15. The transient melting in all the uncapped and capped samples examined in this work exhibited the same characteristic trends.

Dark spots of approximately 5–10 μm size are observed near the center of the heated area. Post-processing microscopy examination using reflected light confirmed that these spots correspond to voids formed in the transient

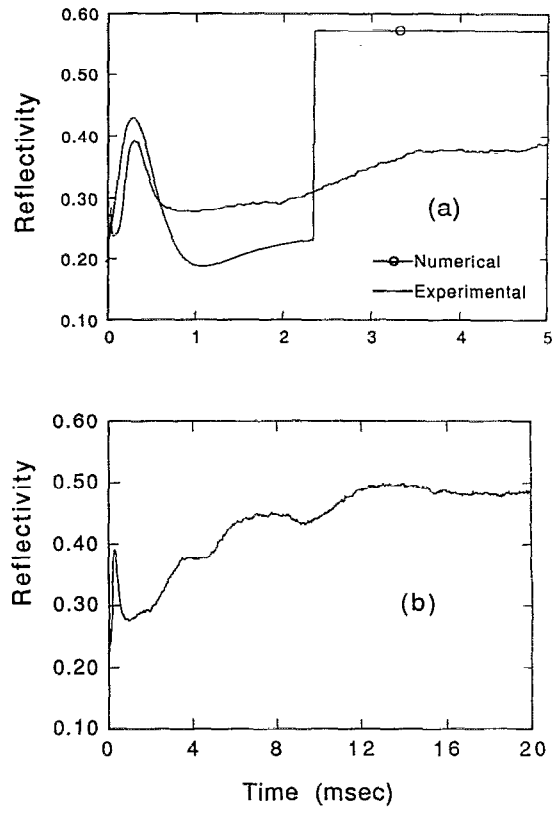

FIG. 15. Comparison between experimental and computed transient reflectivities for the capped, $d_{si}=0.50$ μm, $d_{cap}=0.50$ μm sample, heated by an argon-ion laser beam with $W=60$ μm, $P_T=1.4$ W: (a) over 5 ms and (b) over 20 ms.

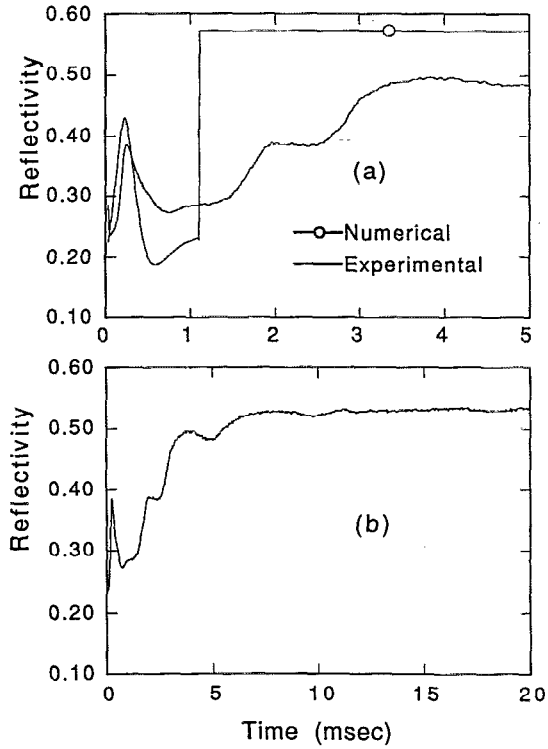

FIG. 14. Comparison between experimental and computed transient reflectivities for a capped, $d_{si}=0.50$ μm, $d_{cap}=0.50$ μm sample, heated by an argon-ion laser beam with $W=60$ μm, $P_T=1.8$ W: (a) over 5 ms and (b) over 20 ms.

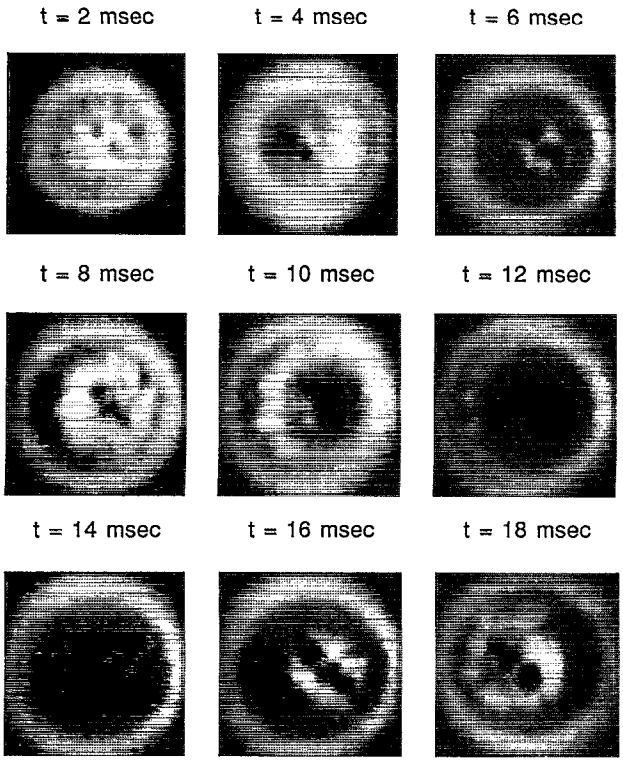

FIG. 16. Sequence of photographs showing the initiation of the phase change process in a capped, $d_{si}=0.5$ μm, $d_{cap}=0.5$ μm, sample. The sample is irradiated by an argon-ion laser beam with $W=60$ μm and $P_T=1.8$ W. Each frame shows a region of approximately 160×160 μm^2.

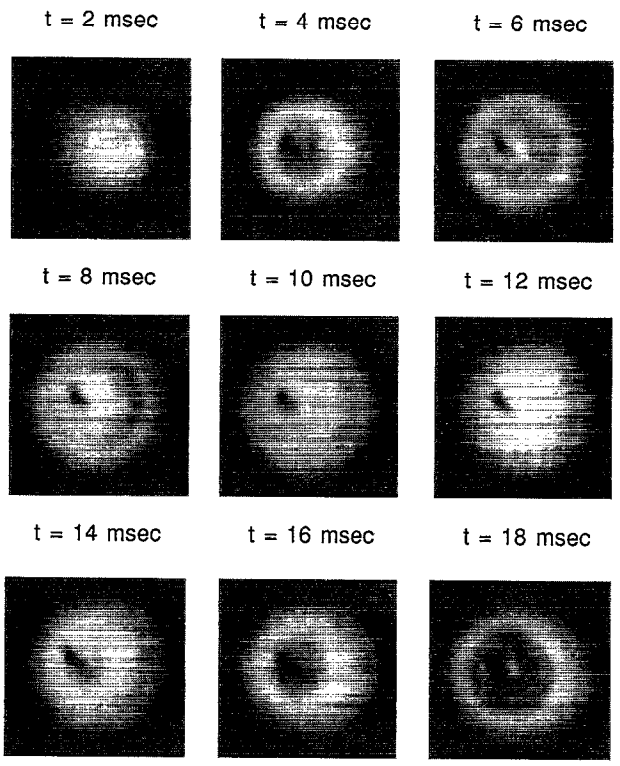

FIG. 17. Sequence of photographs showing the initiation of the phase change process in a $d_{si}=0.5$-μm-thick, capped sample. The sample is heated by an argon-ion laser beam with $W=60$ μm and $P_T=1.4$ W. Each frame shows a region of approximately 160×160 μm^2.

melting process. Such defects have been observed[25] in the "explosive" melting and recrystallization of Si films on patterned SiO_2 using lamp sources. These defects have been attributed[26] to mass transfer in the molten zone, combined with the sudden volumetric contraction of Si upon melting ($\sim$8%), and possibly to the mechanical deformation of the capping layer under the ambient pressure. Surface tension forces in the composite structure of the molten silicon-solid silicon-capping layer-substrate are enhanced because of the thinness of the silicon film, and may also be important in the transient melting process.

IV. CONCLUSIONS

The transient response of thin silicon films during argon-ion laser annealing has been studied. A technique for acquiring localized, *in situ* reflectivity measurements was presented. The spatial resolution achieved is determined by the spot size of the probing HeNe laser beam, and is about 9 μm. Experimentally measured transient surface reflectivities followed the trends obtained by static reflectivity measurements at high temperatures while the material remained in the solid phase. Depending upon the deposition conditions, the optical properties of the thin films may exhibit large deviations from the bulk, single crystalline values. Surface reflectivity measurements were also compared to numerical predictions. The acquired reflectivity signals at the beginning of the phase change process in both capped and uncapped samples exhibit an oscillatory behavior at the millisecond timescale. High-speed photography experiments confirmed the nonhomogeneous periodic nature of the melting process. Recent work[27] includes the detailed experimental investigation of radiative properties of thin semiconductor films at high temperatures.

ACKNOWLEDGMENT

Support to this work by the National Science Foundation, under Grant CTS-9096253, is gratefully acknowledged.

[1] T. I. Kamins, *Polycrystalline Silicon for Integrated Circuit Applications* (Kluwer Academic, Boston, 1988).
[2] R. T. Howe, in *Micromachining and Micropackaging of Transducers*, edited by C. D. Fung, P. W. Cheung, W. H. Ko, and D. G. Fleming (Elsevier, Amsterdam, 1985), p. 169.
[3] R. T. Howe and R. S. Muller, J. Appl. Phys. **54**, 4674 (1983).
[4] G. K. Celler, J. Cryst. Growth **63**, 429 (1983).
[5] B. Y. Tsaur, in *Proceedings of Materials Research Society*, edited by A. Chiang, M. W. Geis, and L. Pfeiffer (MRS, Pittsburgh, PA, 1986), Vol. 53, p. 365.
[6] S. Kawamura, J. Sakurai, M. Nakano, and M. Takagi, Appl. Phys. Lett. **40**, 394 (1982).
[7] K. Kubota, C. E. Hunt, and J. Frey, Appl. Phys. Lett. **46**, 1153 (1985).
[8] C. P. Grigoropoulos, W. E. Dutcher, and A. F. Emery, J. Heat Transfer **113**, 21 (1991).
[9] A. A. Rostami and C. P. Grigoropoulos, *Proceedings of the 1991 ASME Winter Annual Meeting* (ASME, New York, 1991), Vol. HTD-184, p. 53.
[10] C. P. Grigoropoulos, X. Xu, S. L. Taylor, and H. K. Park, in *Proceedings of Materials Research Society*, edited by G. S. Was, L. E. Rehn, and D. M. Follstaedt (MRS, Pittsburgh, PA, 1992), Vol. 235, p. 95.

[11] M. A. Bosch and R. A. Lemons, Phys. Rev. Lett. **47**, 1151 (1981).
[12] R. A. Lemons and M. A. Bosch, Appl. Phys. Lett. **40**, 703 (1982).
[13] R. J. Nemanich, D. K. Biegelsen, and W. G. Hawkins, Phys. Rev. B **27**, 7817 (1983).
[14] C. P. Grigoropoulos, W. E. Dutcher, and K. E. Barclay, J. Heat Transfer **113**, 657 (1991).
[15] M. Born and E. Wolf, *Principles of Optics*, 6th ed. (Pergamon, United Kingdom, 1980), pp. 55, 611.
[16] Z. Knittl, *Optics of Thin Films* (Wiley, Prague, Czechoslovakia, 1976), p. 240.
[17] G. E. Jellison, Jr. and H. H. Burke, J. Appl. Phys. **60**, 841 (1986).
[18] K. M. Shvarev, B. A. Baum, and P. V. Gel'd, Sov. Phys. Solid State **16**, 2111 (1975).
[19] S. Chandrasekhar, A. S. Vengurlekar, V. T. Karulkar, and S. K. Roy, Thin Solid Films **169**, 205 (1989).
[20] T. I. Kamins, J. Electrochem. Soc. **127**, 686 (1980).
[21] G. Harbeke, L. Krausbauer, E. F. Steigmeier, A. E. Widmer, H. F. Kappert, and G. Neugebauer, J. Electrochem. Soc. **131**, 675 (1984).
[22] E. A. Irene and D. W. Dong, J. Electrochem. Soc. **129**, 1347 (1982).
[23] B. G. Bagley, D. E. Aspnes, A. C. Adams, and C. J. Mogab, Appl. Phys. Lett. **38**, 56 (1981).
[24] C. P. Grigoropoulos, A. A. Rostami, X. Xu, S. L. Taylor, and H. K. Park, Int. J. Heat Mass Transfer **36**, 1219 (1993).
[25] D. Dutartre, Appl. Phys. Lett. **48**, 350 (1986).
[26] D. Dutartre, in *Proceedings of Materials Research Society*, edited by J. C. Strum, C. K. Chen, L. Pfeiffer, and P. L. F. Hemment (MRS, Pittsburgh, 1988), Vol. 107, p. 157.
[27] X. Xu and C. P. Grigoropoulos (unpublished).